Open access • Journal Article • DOI:10.1086/522058

Recombination Ghosts in Littrow Configuration: Implications for Spectrographs Using Volume Phase Holographic Gratings — Source link

Eric B. Burgh, Matthew A. Bershady, Kyle B. Westfall, Kenneth H. Nordsieck

Published on: 27 Sep 2007 - Publications of the Astronomical Society of the Pacific (IOP Publishing)

Topics: Spectrograph

Publications of the Astronomical Society of the Pacific, **119**: 1069–1082, 2007 September

Recombination Ghosts in Littrow Configuration: Implications for Spectrographs Using Volume Phase Holographic Gratings

Eric B. Burgh,[1,2] Matthew A. Bershady,[3] Kyle B. Westfall,[3] and Kenneth H. Nordsieck[1]
Received 2007 June 27; accepted 2007 August 2; published 2007 September 27

ABSTRACT. We report the discovery of optical ghosts generated when using Volume Phase Holographic (VPH) gratings in spectrographs employing the Littrow configuration. The ghost is caused by light reflected off the detector surface, recollimated by the camera, recombined by, and reflected from, the grating, and reimaged by the camera onto the detector. This recombination can occur in two different ways. We observe this ghost in two spectrographs being developed by the University of Wisconsin–Madison: the Robert Stobie Spectrograph for the Southern African Large Telescope, and the Bench Spectrograph for the WIYN 3.5 m telescope. The typical ratio of the brightness of the ghost relative to the integrated flux of the spectrum is of order 10^{-4}, implying a recombination efficiency of the VPH gratings of order 10^{-3} or higher, consistent with the output of rigorous coupled wave analysis. Any spectrograph employing VPH gratings, including grisms, in Littrow configuration will suffer from this ghost, although the general effect is not intrinsic to VPH gratings themselves and has been observed in systems with conventional gratings in non-Littrow configurations. We explain the geometric configurations that can result in the ghost, as well as a more general prescription for predicting its position and brightness on the detector. We make recommendations for mitigating the ghost effects for spectrographs and gratings currently built. We further suggest design modifications for future VPH gratings to eliminate the problem entirely, including tilted fringes and/or prismatic substrates. We discuss the resulting implications for the spectrograph performance metrics.

1. INTRODUCTION

Modern astronomical spectrographs are being designed and built to maximize efficiency in all possible ways. CCD quantum efficiencies are nearing 100%, and coatings, both reflection and antireflection, are close to their performance limits as well. The introduction to astronomy of volume phase holographic (VPH) gratings (Barden et al. 2000; Baldry et al. 2004) has further increased routine efficiency by as much as factors of 2.

A VPH grating consists of a thin (3–30 μm) layer of dichromated gelatin (DCG) sandwiched between glass substrates. Through exposure to a laser interferogram, the DCG's refractive index is modulated in a sinusoidal pattern, yielding "fringes," functionally analogous to grooves in a ruled grating, with the principle distinction that the fringes are in a volume not on a surface. With appropriate orientation of the fringe plane, the VPH grating can function in either transmission or reflection. The advantage of VPH gratings relative to conventional surface-relief gratings is their high efficiency (up to 90%), large superblaze (i.e., good efficiency over a broad range of tunable central wavelengths), low scattered light, and transmissivity as well as reflectivity. Transmissivity permits more compact spectrograph designs, particularly for large incidence-angle (i.e., high-dispersion) setups, which allows for more optimum pupil placement, and hence less vignetting. VPH gratings are becoming quite common and are being designed for, or are already being used by, a large number of spectrographs, including some that have been retrofitted with VPH grisms.

The Department of Astronomy and the Space Astronomy Laboratory at the University of Wisconsin–Madison are developing two spectrographs that will also take advantage of this new technology: the Robert Stobie Spectrograph (RSS), formerly called the Prime Focus Imaging Spectrograph, for the Southern African Large Telescope (SALT), and an upgrade for the Bench Spectrograph on the WIYN[4] 3.5 m telescope.

While testing the RSS VPH gratings during the assembly and integration phase, we identified a spurious feature that appeared near the center of the CCD array for all gratings and grating angles (see Fig. 1). We noted that it moved by an angle exactly twice that of any grating rotations off the nominal, Littrow configuration and thus determined that it must arise from a reflection off of, or internal to, the grating. Subsequent measurements during the commissioning of VPH gratings for

[1] Space Astronomy Laboratory, University of Wisconsin–Madison, Madison, WI.

[2] Current address: Center for Astrophysics and Space Astronomy, University of Colorado, Boulder, CO; burgh@colorado.edu.

[3] Astronomy Department, University of Wisconsin–Madison, Madison, WI.

[4] The WIYN Observatory is a joint facility of the University of Wisconsin–Madison, Indiana University, Yale University, and the National Optical Astronomy Observatory.

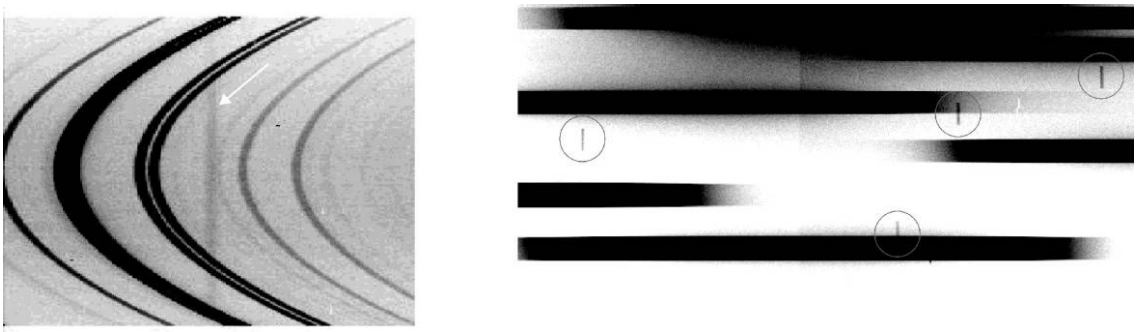

FIG. 1.—*Left*: SALT/RSS detection of Littrow ghost (*straight vertical line in center*) observed in a long-slit arc-lamp spectrum with a 2300 line mm^{-1} grating at $\alpha = 50°$. This is the highest grating angle for RSS, and as such the line curvature is maximal, although in this image the vertical axis has been compressed by a factor of 8 to further accentuate the curvature of the dispersed spectral lines, making the Littrow ghost more obvious. *Right*: Close-up view of Littrow ghosts (*circled*) from a continuum lamp taken through a multiobject slit mask on RSS with a 3000 line mm^{-1} grating at $\alpha \sim 47°$. Each ghost looks like an image of a slitlet on the multiobject slit mask, and is situated opposite the center of field from the Littrow wavelength in its corresponding spectrum (not seen in this figure because of the close-up). Both examples use VPH gratings in first order. Wavelength increases from left to right.

the Bench Spectrograph (see Fig. 2) showed the ghost to not be a feature limited to RSS or one VPH grating manufacturer.

We eventually hypothesized that the ghost was caused by light reflected off of the detector plane, recollimated by the camera, recombined by the VPH grating, and reimaged onto the detector. We called it the "Littrow ghost" because it is a natural consequence of using a grating at Littrow configuration and is not unique to VPH gratings. Although the presence and nature of the ghost has subsequently appeared in the literature (Jones et al. 2004; Saunders et al. 2004), there has been no systematic discussion of its cause, expected amplitude, and paths to mitigating the problem. As it turns out, we have identified two significant ways in which the ghost can arise.

Because the grating can recombine all of the light of the dispersed spectrum that falls on the detector and reimage it into one resolution element, the brightness of the ghost may be high relative to any nearby spectral features, even if the efficiency of recombination by the grating is in the range of 10^{-3}. Therefore, the deleterious effects of the presence of this ghost are significant, especially for multiobject spectroscopy, where each slit will produce a ghost that may not be separated easily from the spectra of objects of interest. Given the substantial efficiency advantages of VPH gratings, it is important to understand the nature of this ghost, and how to use or manufacture such gratings to mitigate or eliminate the effect.

In this paper, we present descriptions of the RSS and WIYN Bench Spectrograph designs and present examples of the ghost. We describe the causes of the ghost and develop a model to predict the position of the ghost and estimate its brightness. Further, we suggest methods for mitigating the effects of this ghost, for gratings already designed as well as for future gratings.

2. UNIVERSITY OF WISCONSIN–MADISON SPECTROGRAPH DEVELOPMENTS

Because the discovery and analysis of the VPH grating ghost was made in the context of two specific spectroscopic instruments, we include here a brief description of their capabilities. These salient attributes contextualize the ghost discussion, and permit a more general interpretation of our examples to other spectroscopic systems. We begin with a basic discussion of spectrographic resolving power, which frames the spectrographs' descriptions, as well as the resulting impact on various modes to mitigate the ghost (§ 4.2).

By equating the size of the entrance slit with that of a spectral resolution element through the appropriate series of transformations, we get the following form for the resolving power:

$$R \equiv \frac{\lambda}{\delta\lambda} = \frac{1}{w}\,\frac{\partial w}{\partial \theta_s}\,\frac{\partial \theta_s}{\partial \alpha}\,\frac{\partial \alpha}{\partial \beta}\,\frac{\partial \beta}{\partial \lambda}\lambda, \tag{1}$$

where $\delta\lambda$ is the size of a resolution element in wavelength; w is the physical slit width; $\partial w/\partial\theta_s$ is the inverse of the telescope scale, relating the slit width to its angular width on the sky, θ_s; $\partial\theta_s/\partial\alpha$ is the angular magnification of the collimator; $\partial\alpha/\partial\beta = 1/r$, where r is the anamorphic magnification; and $\partial\beta/\partial\lambda$ is the angular dispersion of the grating. The angles α and β are the incident and diffracted angles, respectively, at wavelength λ. For a spectrograph with fibers at the entrance rather than a slit at the telescope focal plane, the second two terms would be replaced with $\partial w/\partial\alpha = f_{\rm coll}$, where $f_{\rm coll}$ is the collimator focal length.

For the standard plane-parallel, untilted fringe VPH grating used in the Littrow configuration (i.e., $\alpha = \beta$), this equation reduces to

$$R_{\rm L} = (f_{\rm coll}/w)\,2\tan\alpha. \tag{2}$$

In the case of a fiber-fed spectrograph like the WIYN Bench Spectrograph, w refers to the size of the fiber at the input to the spectrograph. For spectrographs with entrances at the telescope focal plane, like RSS, the slit width relates to the image

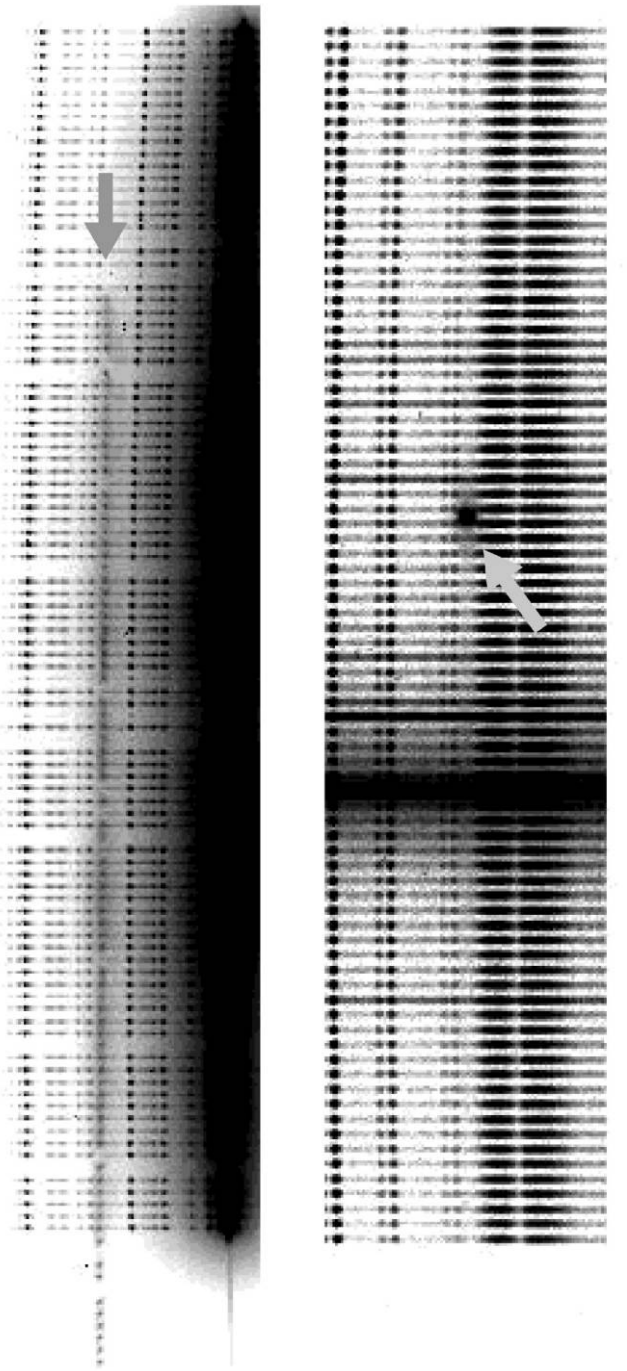

FIG. 2.—Examples of WIYN Bench Spectrograph detection of the Littrow ghost with a 740 line mm^{-1} grating. Only a limited wavelength range is shown. *Left*: Ghosts generated by multiple fibers with roughly equal brightness, using the red Hydra cable and the grating in first order. Gaps, representing broken fibers, illustrate the spatial inversion of the ghost image. The vertical displacement relative to the direct spectrum arises from an out-of-plane misalignment of the grating. *Right*: Ghost generated from a bright source in a single fiber, using the SparsePak IFU and the grating in second order. Wavelength is left to right.

at the telescope focal plane by

$$w = \theta_s f_{\rm coll} (D/d) , \quad (3)$$

where d is the collimated beam diameter, and D is the primary mirror diameter.

2.1. SALT/RSS

The Robert Stobie Spectrograph for the Southern African Large Telescope is a complex spectrograph with multiple operational modes (Kobulnicky et al. 2003) that include long- and multislit spectroscopy and spectropolarimetry. It also contains a double-etalon Fabry-Perot system, developed at Rutgers University (N. Rangwala et al. 2007, in preparation).

The fast beam speed of SALT (F/4.2) and prime focus position of RSS posed great challenges that led to an all-refracting design, incorporating VPH gratings (Burgh et al. 2003). The mechanical design (Smith et al. 2006) of the spectrograph incorporates a camera articulation mechanism and a grating rotation stage for "on-the-fly" repositioning of the camera and grating positions to take full advantage of the tunable blaze properties of the VPH gratings. Articulation angles as high as 100°, and thus incident grating angles in the collimated beam, α, as high as 50°, are possible. With telescope and collimated beam diameters of 11 m and 150 mm, respectively, and a 1.2″ slit, a width well matched to the median image size delivered at the focal plane of SALT, resolving powers as high as 5500 are achieved, following from equation (2).

The RSS grating complement includes five VPH gratings, ranging from 900 to 3000 lines mm^{-1}, fabricated by Wasatch Photonics on fused-silica substrates, and one standard 300 line mm^{-1} surface relief grating from Richardson Gratings. This complement allows for a variety of resolutions and wavelength coverages to be obtained, with maximum resolution achieved in the vicinity of several spectral features of astrophysical importance, such as the Ca II infrared triplet (~850 nm), the Hα region (~650 nm), and the Hβ and O III region (~500 nm).

Multiobject observations with RSS are made using laser-cut carbon fiber masks placed at the 8′ field-of-view focal plane of the telescope. Up to 30 of these custom-cut masks can be installed in a magazine on the spectrograph, so that a wide range of potential science programs are available for observation on any given night—well suited to the intrinsically queue-scheduled nature of the telescope.

2.2. WIYN Bench Spectrograph

The WIYN Bench Spectrograph (Barden et al. 1993, 1994) is bench-mounted, fiber-fed, and situated in a climate-shielded room two stories below the telescope observing floor. Feeds for the 75 mm spectrograph slit include two 100 fiber MOS cables (Hydra) with access to 1 deg^2 on the sky, and two IFUs (DensePak and SparsePak) covering a 0.3′–1′ field of view. Fibers are 200–500 μm in diameter, or roughly 1.8″–4.6″ at the F/6.3 Nasmyth focus of the telescope (8.8″ mm^{-1}). Performance

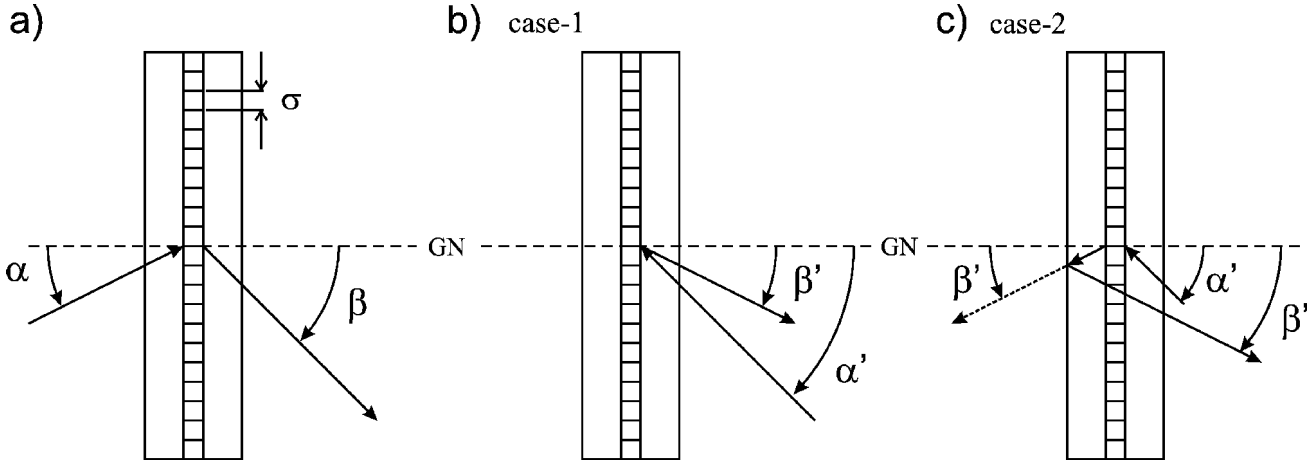

FIG. 3.—(*a*) In-plane (i.e., $\gamma = 0$) geometry for first (transmissive) pass through a plane-parallel VPH grating (not to scale). (*b*) Geometry for case 1 ghost: reflection off of the grating (β') after reflection off of the CCD and recollimation by the camera (α'). (*c*) Geometry for case 2 ghost: transmission through the grating (α'), again after CCD reflection and camera recollimation, then reflection off the substrate air-glass interface, and finally zeroth-order grating transmission (β'). Angles are measured relative to the grating normal (GN). Note that the refractive changes of angles at the substrate interfaces have been ignored (see text).

features of the system with SparsePak are presented in Bershady et al. (2005).

The spectrograph consists of an on-axis parabolic reflecting collimator ($f_{\rm coll} = 1021$ mm), one or two grating turrets, and an all-refractive camera.[5] The spectrograph can be optimized for a wide range of gratings (echelle and low-order surface-relief gratings, as well as VPH) because of its adjustable camera-collimator, grating, and CCD focal-plane angles, as well as adjustable grating-camera distance. Double-turret configurations allow for a fold-flat to accommodate small grating angles, or a second grating. In contrast to RSS, only the grating angle of the primary is currently remotely controllable, with the remaining degrees of freedom requiring manual adjustment.

In Littrow, single-grating configurations, the Bench achieves $R = 17{,}800$ at $\alpha = 50°$ for a 1.2″ effective slit width. At comparable grasp ($A\Omega$) with RSS on SALT (scaling from respective clear apertures of 60 and 8 m^2), the Bench achieves $R = 6500$ (3.3″ effective slit width), or 15% higher than RSS. However, the Bench can be used at higher angles, with VPH gratings optimized for α as large as 70° now being implemented; in non-Littrow configurations (e.g., a 316 line mm^{-1} echelle blazed at 63.4°) yielding anamorphic demagnification factors that boost R by factors of 40%–50%, and in double-grating configurations where one or both gratings have transmissive diffraction. Reported here are the results of a 740 line mm^{-1} VPH grating developed by Sam Barden with CSL (Centre Spatiale de Liege), made on float-glass and postpolished to 60% Strehl at Lawrence Livermore Labs via NOAO contract, and implemented on the Bench at low angles of 17°–24° via a double-turret configuration using a fold-flat in the primary turret.

[5] A second, catadioptric camera can be used for low-dispersion work into the blue, but is lossier because of a central obstruction filled in by fiber focal ratio degradation.

3. GHOST MODEL

Based on the appearance of ghost images in two independent spectrographic systems, we have constructed a physical model that allows us to reproduce their behavior and predict a more general ghost phenomenon. The incident light is dispersed by the transmission grating and is focused onto the CCD by the camera. A sizable fraction of the light, roughly 10% (perhaps even higher at wavelengths where the QE is low), is reflected from the surface of the CCD and recollimated by the camera. On reaching the grating, it is recombined and reflected back through the camera on a third pass. Depending on the order of interaction with the grating, this may result in an image of the spectrograph entrance focal plane or another spectrum with (possibly) different dispersion on the detector plane.

There are two paths for this recombination: (1) dispersive (i.e., nonspecular) reflection off of the grating back toward the camera (see Fig. 3*b*; we refer to this as case 1 or "reflective" ghost); or (2) dispersive transmission through the grating, then reflection off of the air-glass interface of the grating substrate on the far side, followed by a zeroth order transmission back through the grating, sending the light in the direction of the camera (see Fig. 3*c*; we refer to this as case 2 or "transmissive" ghost). Both recombination paths produce essentially the same effect for plane-parallel gratings substrates and untilted fringes, although in general they have different efficiencies, and do not share the same set of solutions (§ 4).

To understand how these ghost mechanisms work in quantitative detail, we start with the generalized grating equation,

given by

$$m\lambda = n_i\sigma(\sin\alpha_i + \sin\beta_i)\cos\gamma_i, \tag{4}$$

where n_i is the index of refraction of the medium,[6] α_i is the incident angle of the light relative to the grating normal in the plane perpendicular to the grating grooves, β_i is the diffracted angle for order m, σ is the groove spacing, and γ_i is the incident angle in the plane parallel to the grooves. This holds for passage through the DCG ($i = 2$), the substrate material ($i = 1$), or the air ($i = 0$). For the sake of simplicity we will, unless specified otherwise, refer to the angles in air and use the angles without subscripts, i.e., $\alpha = \alpha_0$, etc. See Figure 3*a* for a schematic representation of this geometry.

On the light's first pass through the grating, the output angle is then

$$\sin\beta = \frac{m\lambda}{\sigma\cos\gamma} - \sin\alpha. \tag{5}$$

The dependence of β on γ is what is responsible for spectral line curvature, as seen in Figures 1 and 2.

After reflection from the detector surface and subsequent recollimation by the camera, the light interacts with the grating again, with an output angle following

$$\sin\beta' = \frac{m'\lambda}{\sigma\cos\gamma'} - \sin\alpha'. \tag{6}$$

Note that for generality we have allowed the second diffraction to be in another order. For the case in which the surface of the grating substrate is parallel to the grating, the output angle is the same after reflection from the substrate air-glass interface, and thus this equation holds for both the reflective and transmissive recombinations (see Figs. 3*b* and 3*c*, respectively).

Because the reflection off the detector happens at a focus, where the position on the detector is conjugate with angle in the collimated beam, the angle that the light makes as it is recollimated will be the same as it was after dispersion. Therefore, the incident angle for the second encounter with the grating is equal to the diffracted angle after the first, i.e., $\alpha' = \beta$, and thus

$$\sin\beta' = \frac{m'\lambda}{\sigma\cos\gamma'} - \left(\frac{m\lambda}{\sigma\cos\gamma} - \sin\alpha\right). \tag{7}$$

Because $\cos\gamma' = \cos\gamma$, this reduces to

$$\sin\beta' = \frac{\Delta m\lambda}{\sigma\cos\gamma} + \sin\alpha, \tag{8}$$

where $\Delta m \equiv (m' - m)$. The angular dispersion of the ghost will be

$$A' = \frac{\partial\beta'}{\partial\lambda} = \frac{\Delta m}{\sigma\cos\beta'\cos\gamma}. \tag{9}$$

Because the angular dispersion of the direct spectrum is $A = m/(\sigma\cos\beta\cos\gamma)$, the relative dispersions between the direct and the ghost spectra for $\beta' = \beta$ will be

$$A'/A = \Delta m/m. \tag{10}$$

It follows from equations (8) and (10) that an important parameter for determining the position and dispersion of the ghost is Δm, the relative change in order of the ghost to the direct spectrum. A few interesting cases are presented in the following sections.

3.1. Ghost Modes

3.1.1. Narcissistic Ghost ($m' = 0$)

The trivial case where $m' = 0$ produces a "narcissistic" ghost. In this case, the grating acts as a mirror, i.e., $\beta' = -\alpha'$, and the ratio of the dispersions will be $A'/A = -1$, resulting in an inverted spectrum. In the case of VPH gratings, it may be likely that a simple reflection off of the air-glass interface of the camera-side substrate produces this ghost with more efficiency than a zeroth-order reflection from the DCG. This case is particularly harmful when $\beta = 0$ (McCandliss et al. 1998), or when β is less than the viewing angle of the camera.

3.1.2. Littrow Ghost ($\Delta m = 0$)

If the recombination by the grating is in the same order as the initial diffraction, then $\Delta m = 0$. Equation (8) is then simply $\beta' = \alpha$, and the light follows the path of the Littrow wavelength, independently of wavelength, i.e., the light is fully recombined. This results in an image of the spectrograph entrance slit(s), *without line curvature*, on the detector at the location of the Littrow wavelength, as illustrated in Figures 1 and 2.

VPH gratings are most efficient near the Bragg wavelength, i.e., when the light is "reflected" from the plane of the grating fringes:

$$\alpha_2 - \phi = \beta_2 + \phi, \tag{11}$$

where α_2 and β_2 are the angles of incidence and reflection, respectively, inside the DCG, and ϕ is the tilt of the fringes relative to the grating normal (see Fig. 5). For a grating with untilted fringes,[7] i.e., $\phi = 0$, like the ones built for RSS and the WIYN Bench Spectrograph, this results in the highest efficiencies being produced at the Littrow condition, i.e., $\alpha_2 = \beta_2$. For a plane-parallel grating, the DCG is sandwiched be-

[6] In this work we ignore any wavelength dependence of the index of refraction.

[7] The general case, which includes tilted fringes, is discussed in § 4.2.

tween flat substrates, and it also holds that $\alpha = \beta$. Thus, the standard operating mode is in this Littrow configuration and the central wavelength on the detector is the "Littrow wavelength," defined as

$$\lambda_L = (2\sigma \sin \alpha)/m. \quad (12)$$

Because this is the standard configuration, VPH spectrographs are particularly sensitive to the Littrow ghost.

Since the camera-collimator angle, Φ, is equal to $\alpha + \beta'$ for the ghost, $\Phi = 2\alpha$ and $d\Phi/d\alpha = 2$, i.e., when the grating is moved by $\delta\alpha$ away from a Littrow configuration, the ghost moves twice that angle, consistent with what was observed.[8]

3.1.3. Other Recombinations

In the case that $\Delta m \neq 0$, the light will not fully recombine, and the ghost will take the form of a spectrum. The zeroth order, $m' = 0$, results in the "narcissistic" ghost described above, but for gratings that operate at second order or higher there exists the possibility of other ghosts.

In general, the configurations that will result in the production of this ghost are ones in which the ghost is in a Littrow configuration, and thus the recombined light follows the direction of the primary spectrum, i.e., $\sin \beta' = \sin \beta$. Combining equations (5) and (8) produces the wavelengths at which this will occur:

$$\lambda = \frac{2(\sigma/m) \sin \alpha}{1 - \Delta m/m} = \frac{\lambda_L}{1 - \Delta m/m}, \quad (13)$$

where λ_L is the Littrow wavelength (eq. [12]) for the given grating's line ruling, angle, and order of primary use. Solutions only exist for $\Delta m/m < 1$, so $m' < 2m$.[9] Thus, only gratings in second order or higher can see this "cross-order" ghost. What is observed is a partially recombined ghost spectrum ($\Delta m/m < 1$), which may be inverted in wavelength ($\Delta m < 0$) or not ($\Delta m > 0$) as per equation (10), having the above wavelength in common with the direct spectrum.

In practice, this type of ghost is of relevance to primary spectra produced in off-Littrow configurations that may include light at significant power in the Littrow wavelength for another order. While existing VPH gratings are designed to work in Littrow, they can be used off-Littrow. Future gratings with tilted fringes (§ 4.2.1) will also operate in non-Littrow configurations, where this ghost may arise if used in second or higher order. Furthermore, a "cross-order" ghost was observed in the Gemini Near-Infrared Spectrometer (GNIRS; Joyce 2003) using surface-relief reflection echellettes, demonstrating that our general ghost model is not intrinsic to VPH gratings nor to the use of a primary Littrow configuration.

In the GNIRS case, a 110.5 line mm^{-1} surface-relief reflection grating, blazed for 6.79 μm in first-order Littrow, was used at $\alpha = 39.1°$ and $\beta = 12.1°$ in second order ($m = 2$). This yields a central wavelength of 3.8 μm. A Littrow configuration for the ghost, $\beta' = \beta = 12.1°$, also occurs at 3.8 μm for a first-order reflection ($m' = 1$), following directly from equation (13) (with $\lambda_L = 5.7$ μm for this grating at $m = 2$ and $\alpha = 39.1°$). The result is fully consistent with what they noted: the ghost's resolving power was half the primary spectrum, and the length of the ghost was exactly half of the detector width. These effects arise because the relative change in dispersion will be, according to equation (10), $A'/A = -1/2$, and only the wavelengths in the primary spectrum will contribute. Should the grating have significant efficiency across multiple orders for a given wavelength, more ghosts, at wavelengths satisfying equation (13), may be observable. Indeed, this is the case for the GNIRS grating suite, and Joyce (2003) mentions having observed ghosts in other configurations.

3.2. Off-Axis Ghosts and Multiobject Spectroscopy

For spectrographs that employ a single entrance slit, or have a fiber bundle aligned as a long slit, like the WIYN Bench Spectrograph, the Littrow ghost will be constrained to a single area on the detector (see left panel of Fig. 1 or Fig. 2). However, for a multiobject spectrograph like RSS, which uses multiple apertures at the focal plane, ghosts arise from the spectra through each aperture.

For light that arrives at the grating off-axis[10] in the spectral dimension by an amount $\Delta\alpha$, the diffracted angle is

$$\sin \beta = \frac{m\lambda}{\sigma \cos \gamma} - \sin (\alpha + \Delta\alpha), \quad (14)$$

and following the same steps as for the on-axis case (eqs. [5] and [6], i.e., a reflection) results in a ghost angle of

$$\sin \beta' = \frac{\Delta m\lambda}{\sigma \cos \gamma} + \sin (\alpha + \Delta\alpha). \quad (15)$$

For the Littrow ghost, $\Delta m = 0$, and

$$\beta'_L = \alpha + \Delta\alpha, \quad (16)$$

resulting in a ghost positioned opposite the center of field from its Littrow wavelength in the primary spectrum (the mirroring

[8] An interesting side note is that this sensitivity of the ghost position can be utilized as a calibration of the grating rotation angle. For RSS, the ghost moves one unbinned pixel per 4.5″ of grating rotation.

[9] In principle, the order for the ghost is further constrained by the fact that the wavelength must be diffracted by an angle less than 90° for the first pass through the grating, so $\sin \beta < 1$. The result is that $m' < 2m/(1 + \sin \alpha)$. In practice, it will be even more constrained by the fact that the wavelength must fall on the detector to be reflected in the first place, i.e., $\beta_c + \delta > \beta > \beta_c - \delta$, where β_c is the angle of the central wavelength and δ is the camera half-angle field of view.

[10] An object that is off-axis by an angle x in the focal plane field of view will have an optical magnification equal to the ratio of the focal lengths of the telescope and spectrograph collimator and arrive at the grating off-axis by $\Delta\alpha = xf_{tel}/f_{coll}$.

is in both dimensions). Each aperture in the slit mask will have such a ghost (see right panel of Fig. 1), and thus the overall effect is an image of the focal plane on the detector mirrored through the optical axis.

3.3. Recombination-Ghost Efficiency of VPH Gratings

Here we focus on the fully recombined $\Delta m = 0$ Littrow ghost, but our development is general in the context of the integrated ghost flux. The detected integrated brightness of the ghost will be

$$B = \int_{\lambda_1}^{\lambda_2} F(\lambda) R_{\rm CCD}(\lambda) T_{\rm cam}^2(\lambda) \epsilon_{m'}(\lambda)\, d\lambda, \qquad (17)$$

where $F(\lambda)$ is the impinging flux of the direct dispersed spectrum on the CCD; $R_{\rm CCD}$ is the CCD reflectivity; $T_{\rm cam}$ is the throughput of the camera, including the reflective losses at the camera-side grating-substrate air-glass interface (squared because there are two passes); $\epsilon_{m'}$ is the recombination efficiency of the grating in order m', and λ_1 and λ_2 are the lower and upper wavelengths that impinge on the CCD(s) in the primary spectrum.

In the case 1 reflective recombination ghost, $\epsilon_{m'}$ will be $\epsilon^R_{m'}$, the reflective diffraction efficiency in order m'. In the case of the transmissive recombination, the efficiency is

$$\epsilon_{m'} = \epsilon^T_{m'} R_{\rm sub} \epsilon^T_0, \qquad (18)$$

where $\epsilon^T_{m'}$ is the transmission efficiency in order m', $R_{\rm sub}$ is the reflectivity of the substrate air-glass interface, and ϵ^T_0 is the zeroth order transmission efficiency of the grating.

In the extreme case where $R_{\rm CCD} = 1$ and $T_{\rm cam} = 1$, we would expect the lower limit for the efficiency, $\epsilon_{m'}$, of the grating recombination to be of the same order as the ratio of the integrated flux in the ghost to the integrated flux of the direct spectrum. For RSS and the Bench, this ratio is typically observed to be a few times 10^{-4}. With CCD reflectivities in the 10% range and more realistic camera throughputs, the efficiency, $\epsilon_{m'}$, would be at least a few times 10^{-3}.

Figure 4 shows the efficiencies of the transmissive and reflective recombinations, estimated for one particular RSS grating configuration (2300 line mm^{-1} grating used at $\alpha \sim 37°$) using a rigorous coupled-wave analysis code (RCWA).[11] We show a range of efficiencies for the transmissive recombination (case 2), corresponding to substrate air-glass interface reflectivities of 0.5%–2%, and assuming that the zeroth order transmission is equal to 1 minus the first-order transmission ($\epsilon^T_0 = 1 - \epsilon^T_1$), an assumption supported by the RCWA results. For this recombination case, ϵ is in the few times 10^{-3} range, consistent with that observed, and factors of a few more efficient than the reflective recombination (case 1) ghost.

[11] RCWA code, written in C, was generously provided by Gary Bernstein, who implemented the methods of Moharam & Gaylord (1983).

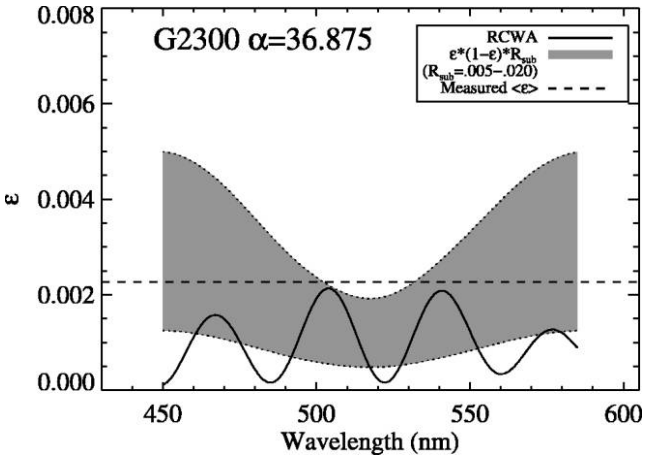

FIG. 4.—Efficiencies of reflective and transmissive recombination for a specific RSS grating configuration, as defined in the text. The solid line is the RCWA prediction for the first-order reflection efficiency. The shaded region shows the predicted efficiency of the transmissive ghost, with lower and upper bounds on the substrate reflectivity of 0.5%–2%. Note that reflective losses from the camera-side substrate air-glass interface, which will be the same for both cases, are not included. The dashed line is the measured average value of the recombination efficiency for this grating configuration as derived from $\epsilon = (B/F_d)/(T^2_{\rm cam} R_{\rm CCD})$, which follows from eq. (17), where B and F_d are the integrated fluxes of the ghost and direct spectrum, respectively, $T_{\rm cam}$ is the measured camera throughput of RSS, and where we have assumed that $R_{\rm CCD}$ is $1 - QE_{\rm CCD}$, i.e., no absorption.

The brightness of the case 2 recombination will depend on the performance of the antireflection coating, which in turn will depend on the particular coating recipe and incident angle. In most cases, we believe the reflectivities should be in our adopted range, and although the case 2 ghost may be the brighter one in general, we do expect that both ghost production methods will contribute to the overall intensity of the ghost. If, however, the grating is designed for use at very large incidence angles ($\alpha > 50°$), such as used on the Bench, the case 2 ghost could be significantly stronger than the case 1 ghost. Because of their different response to mitigation (§ 4), it is important to track both cases.

For the $\Delta m = 0$ ghost, there is complete recombination, and the relative brightness of the ghost to the direct spectrum is enhanced by the number of resolution elements on the detector, which in modern spectrographs can be as high as 10^3 (see eq. [27]). Therefore, the flux of the ghost may be a significant fraction of the flux per resolution element of the direct spectrum, and, depending on the character of the direct spectrum and the placement of the ghost, the ghost may actually be brighter than its surroundings. This is seen in Figures 1 and 2.

4. GHOST MITIGATION

The discovery of this ghost was unexpected. Through testing and on-sky observations it has become clear that it can be bright enough to cause significant disruption of the primary data. In the following sections we describe potential methods for min-

imizing the effects of the ghost for both existing and future spectrographs.

4.1. Existing Gratings

In spectrographs that have already been designed and built to use VPH gratings, there are several options to limit the effects of the ghost.

4.1.1. Off-Littrow Configurations

As mentioned in § 3.1.2, the ghost moves when the grating angle is changed. However, for a fixed camera-collimator angle, $\Phi = \alpha + \beta$, the central wavelength on the detector, to zeroth order, does not move with grating tilt. This follows from

$$\frac{d\Phi}{d\alpha} = 1 + \frac{\partial\beta}{\partial\alpha} = 1 - \frac{\cos\alpha}{\cos\beta}, \tag{19}$$

and the fact that near Littrow $\alpha \approx \beta$, so $d\Phi/d\alpha \approx 0$.

Consequently, the position of the ghost can be moved with small movements of grating angle, and subsequent small changes in central wavelength and dispersion. For a single-slit spectrograph, to move the ghost completely off the detector requires a grating rotation of $\Delta\alpha = \delta/2$, where δ is the camera half-angle field of view in the dispersion direction.[12] For detectors with CCD mosaics, like the three-chip RSS detector, the gap between chips may provide a convenient place to put the ghost, which can be accomplished with a smaller grating rotation. For a multiobject spectrograph, the rotation will need to be larger, to accommodate the off-axis ghosts as well.

The downside to such a maneuver is that the VPH blaze efficiency is shifted when operated off-Littrow, and the change in efficiency may be significant even for small moves such as that needed to put the ghost in the detector gap for a single-slit spectrograph. For example, the RSS camera has a half-angle FOV of $\delta \sim 8°$, requiring a grating rotation of $\Delta\alpha = \delta/2 = 4°$ to remove the ghost completely ($\Delta\alpha = 2.4°$ for the Bench); however, it is a 3 chip mosaic, so to put the ghost in the detector gap would only require a move of $\Delta\alpha = (\delta/3)/2 = 1.33°$. For a typical RSS or Bench grating configuration, going off-Littrow by this amount produces a blaze shift that can reduce the efficiency at one end of the spectrum by as much as ~20% (with a corresponding increase at the other end). In practice, the details of the blaze shift will depend on the grating and the grating angle.

In multiobject mode, the grating would have to be tilted even farther to accommodate the ghosts generated by off-axis slits. For RSS as much as an additional 2.5° of grating rotation could be necessary to remove all ghosts from the detector, depending on the distribution of slitlets on the multiobject slit mask.

[12] Camera FOV $= 2\delta = \arctan(d/f_{\rm cam})$, where d is the detector size in the dispersion direction and $f_{\rm cam}$ is the camera focal length.

4.1.2. Out-of-Plane Configurations

Another option would be to have the grating placed out-of-plane, i.e., $\gamma \neq 0$ for on-axis light. To move the ghost completely off the detector may then require a smaller angle out-of-plane than the in-plane, off-Littrow configuration if the detector is wider in the dispersion direction. For example, the RSS detector array has a 1.5 aspect ratio, so the half-angle field of view in the spatial direction is $\frac{2}{3}$ the value of the spectral direction, or about 5.33°. The corresponding value for the Bench, given the 2 : 1 aspect ratio of the used portion of the CCD, is 2.4°. An out-of-plane tilt of the grating of this amount would move the entire ghost off the detector, for both long-slit and multiobject modes. For a given β, there may be no resulting blaze shift; however, the center of the line curvature will shift, resulting in a potentially substantial enhancement of line curvature on one side of the spectral lines. The practicality of implementing this configuration will depend on the spectrograph. For example, it is relatively straightforward to modify the grating mounts on the Bench, but strong mechanical constraints prohibit this on RSS.

4.1.3. Dithering

In practice, we postulate that the best method for mitigating the effects of the ghost is procedural, achieved by employing a "dithering" procedure, in which an observation is split into two (or more) exposures, each with a different instrument physical configuration. There are three potential spectrograph dither types: the camera-collimator angle, Φ, is kept the same, but the grating angle, α, is changed to an off-Littrow configuration; α is kept the same, but Φ changed; or both angles are changed such that a Littrow configuration is maintained. An additional form of dithering would be to maintain a fixed spectrograph configuration, but nod the telescope so that the object of interest occupies a different position along the slit.

1. *Grating rotation only*.—In this case, the position of the ghost will move by twice the grating angle change, as described in § 3.1.2, with little to no change in position of the primary spectrum (see eq. [19]). However, the dispersion of the primary spectrum will change somewhat by such a grating rotation, making it difficult to simply co-add the two exposures and requiring independent wavelength and/or flat-field calibrations. As mentioned above, the move to an off-Littrow configuration will shift the blaze; however, if the goal is to only move the ghost by a resolution element or two, the shift is negligible. This option may work best for spectrographs like the WIYN Bench Spectrograph, for which the camera-collimator angle may not be changed during the course of an observation, but grating angle can.

2. *Camera-collimator angle change only*.—A change in Φ may be desirable in a CCD mosaic in order to recover any wavelength coverage lost in the detector gaps. If this were done, with fixed grating angle, the central wavelength would be dif-

ferent. However, with no change in α, the Littrow ghost will continue to follow the path of the Littrow wavelength, i.e., the ghost shifts the exact same amount as the direct spectrum, and no separation between the two is achieved. In short, this approach does not work.

3. *Maintain Littrow configuration*.—Perhaps the best solution for spectrographs like RSS, which allow for remote control of both α and Φ, is to adjust both while maintaining a Littrow configuration. This results in movement of the direct spectrum, because of the change in Φ, so that the wavelengths that fall in the detector gaps are recovered; it also results in the movement of the ghost, because of the change in α. However, as in option (1) above, additional calibration and wavelength solutions are needed, and no simple co-addition of the data is possible.

4. *Telescope nod*.—While maintaining a fixed spectrograph configuration, a telescope nod can be performed to place the object of interest at different spatial positions along the slit. This either moves the ghost relative to the source (source-limited regime; see Fig. 2, *right panel*), or moves the source to intersect the ghost at a different wavelength (background-limited regime; see Figs. 1 or 2, *left panels*). In general, the feasibility of this solution depends on the spatial extent of the source, and the degree of line curvature in the spectrum. The advantage of this approach is that it requires no additional instrument setup or calibration.

Each of the three methods (1), (3), and (4) will mitigate the effect of the ghost overlapping an area of interest in the direct spectrum; however, the extent to which each is desirable depends on the specific science goals of the observation and the technical limitations of the telescope/spectrograph system (i.e., the cost and feasibility of multiple calibrations). If continuous wavelength coverage is of high importance for multidetector systems such as RSS (where detector gaps are present), then methods (1) and (3) would be best. They require the additional overhead associated with both the reconfiguration of the spectrograph as well as the need to recalibrate the reconfigured system. Otherwise, method (4) is likely the most natural solution, because it is often the case that one wishes to dither a source along the slit (to minimize or average slit or detector variations and defects).

Since method (4) has some clear operational advantages, we elaborate under what conditions it will work. In all cases when the ghost is dominated by flux from the source, and the source is small relative to the slit length, the ghost's discrete image in the spatial dimension (along the slit) is reflected about the center of the detector (barring any out-of-plane grating misalignments). Consequently, a maneuver to position the source off-axis will move the ghost by an equal amount in the opposite direction (see right-hand panel of Fig. 2, where the ghost is offset from its direct spectrum). For point-source objects, where the spectrum (and hence ghost) is source-limited, small nods would suffice, with little to no impact on the wavelength coverage, dispersion, or line curvature.

For background-limited observations, the ghost is generated predominately by the sky lines and thus is uniform in intensity at all slit positions (corrected for vignetting). Small nods do not move the direct spectrum away from the ghost. However, at high enough grating angle, one may take advantage of the line curvature to place the source at two slit locations that have the ghost intersection with the direct spectrum at different wavelengths. Line curvature follows from differentiating equation (5) with respect to γ:

$$\cos\beta\,\frac{\partial\beta}{\partial\gamma} = \frac{m\lambda}{\sigma}\,\frac{\tan\gamma}{\cos\gamma}. \tag{20}$$

At the Littrow wavelength (eq. [12]) and for small values of γ, this reduces to

$$\frac{\partial\beta}{\partial\gamma} = 2\gamma\tan\alpha, \tag{21}$$

which gives

$$\beta_{\gamma} = \gamma^2\tan\alpha, \tag{22}$$

where β_{γ} is the change in β from that for the Littrow wavelength on the optical axis, $\gamma = 0$. The spectral lines are curved parabolically and shift to higher angles, i.e., longer wavelengths, along the slit.

The minimum movement necessary would be one that changes the diffracted angle by an amount equal to that for a resolution element, which in terms of β follows from the generalized resolving power equation (eq. [1]) and can be written as

$$\delta\beta = w\,\frac{\partial\theta_s}{\partial w}\,\frac{\partial\alpha}{\partial\theta_s}\,\frac{\partial\beta}{\partial\alpha} = \frac{wr}{f_{\rm coll}}. \tag{23}$$

At Littrow, the anamorphic factor, r, equals 1. Setting the above equation equal to equation (22) and solving for γ produces

$$\gamma = \sqrt{w/(f_{\rm coll}\tan\alpha)}, \tag{24}$$

which, in terms of the filled-slit resolving power at Littrow (eq. [2]), can be written as

$$\gamma = \sqrt{2/R_{\rm L}}. \tag{25}$$

This angle is measured in the collimated beam and can be related to the on-sky angle in the spatial direction, θ, by $\gamma = \theta f_{\rm tel}/f_{\rm coll}$. For RSS at the highest resolving powers, (i.e., $R_{\rm L} = 5500$ for $\alpha = 50^\circ$ and $\theta_s = 1.2''$), this amounts to a minimum of $\sim 1'$ nod. For the lowest resolving power settings ($R_{\rm L} \sim 1000$), the nod would be about twice as large.

4.1.4. VPH Grisms

It should be noted that a ghost should appear in VPH grism spectrographs as well; however, we expect only the reflective recombination ghost to contribute. In the transmissive recombination case, the light would not be redirected into the camera because of the typically large prism angles in a grism.

The Low Resolution Spectrograph for the Telescopio Nazionale Galileo has reported observing a ghost while commissioning new VPH grisms in late 2005.[13] A ghost has also been seen in the new grism for the Andalucia Faint Object Spectrograph and Camera on the Nordic Optical Telescope.[14] As reported, these ghosts match well the model discussed in this work.

In the case of grism spectrographs, where zero-deviation configurations are implemented, it is not possible to change the grism configuration between exposures. One would have to move the position of the object on the telescope focal plane, either by nodding the telescope along the slit axis, as mentioned in the previous section, or by repositioning the slit in the dispersion direction (with accompanying shift in central wavelength), which some grism spectrograph designs can accommodate. Because the ghost is reflected about the optical axis, the former case would separate the object and ghost in the spatial direction and the latter in the spectral direction.

4.2. Future Gratings

Given the freedom to design a VPH spectrograph with the foreknowledge of the Littrow ghost, there are ways to mitigate the problem by modifying the grating design. The possibilities include tilting the fringes and/or applying a wedge to the grating substrates. The concept of fringe-tilting in plane-parallel VPH gratings to remove the Littrow ghost is mentioned in Saunders et al. (2004), while Baldry et al. (2004) describe prismatic substrates for VPH gratings, although not in the context of ghost removal. Figure 5 shows the geometry for a generalized VPH grating with both tilted fringes and wedged substrates. We consider only cases in which the two substrates have the same index of refraction.

In addition to mitigating the ghost problem, redesigning the grating can have an impact on the resolving power and the number of resolution elements, and so we consider these two information metrics in tandem. For this discussion, we refer back to equation (1), the generalized form for the resolving power. The first three terms, $(1/w) \times \partial w/\partial\theta_s \times \partial\theta_s/\partial\alpha$ $(= f_{\rm coll}/w)$, represent the fixed geometry for a given spectrograph collimator and slit width, and remain constant for all grating configurations. The final three terms depend on the geometry of the grating setup, however, and we define this as the resolution merit function $(1/r) \times d\beta/d\log\lambda$, following Bershady (2007).

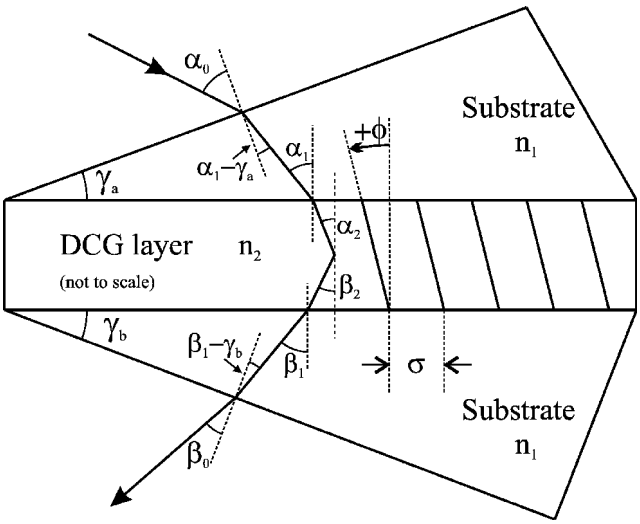

FIG. 5.—General geometry for prism-immersed VPH grating with tilted fringes. For tilted fringes only, $\gamma_a = \gamma_b = 0$. For prism immersion only, $\phi = 0$. In general, the two substrate refractive indices can be different.

Evaluating at the Bragg wavelength, this merit function takes the form

$$\frac{1}{r}\frac{d\beta}{d\log\lambda} = \frac{\cos(\alpha_1-\gamma_a)}{\cos\alpha_1}\,\frac{\sin(\alpha_2-\phi)}{\cos\alpha_0}\,2n_2\cos\phi, \quad (26)$$

where the internal angles relate to each other through Snell's law: $\sin\alpha_0 = n_1\sin(\alpha_1-\gamma_a)$ and $n_1\sin\alpha_1 = n_2\sin\alpha_2$ (see Fig. 5).

It can be shown for the plane-parallel grating,[15] using equation (1), that the number of resolution elements on the detector is

$$N_R = \frac{\Delta\lambda}{\delta\lambda} = \frac{2\sin\delta}{r}\,\frac{f_{\rm coll}}{w}, \quad (27)$$

where $\Delta\lambda$ is the full wavelength coverage on the detector.

The following sections discuss two cases, those of a plane-parallel, tilted fringe grating, and a prism-immersed, untilted fringe grating.

4.2.1. Tilted Fringe Gratings

In this section, we consider plane-parallel gratings ($\gamma_a = \gamma_b = 0$) with tilted fringes ($\phi \neq 0$). We define the sign of the tilt such that positive tilts move the plane of the fringes toward the incident beam and decrease β, while negative tilts move away and increase β (see Fig. 5). These gratings would be most efficient at the Bragg wavelength, not the Littrow wavelength, and hence would be used in an off-Littrow configuration. With

[13] See http://www.tng.iac.es/news/2005/12/13/lrs−vph/.

[14] See http://www.not.iac.es/instruments/alfosc/grisms/grism17.html.

[15] After noting that $\Delta\lambda = 2(\sigma/m)\cos\beta\sin\delta$.

a nonzero fringe tilt, the Bragg wavelength, λ_B, is found to be

$$\lambda_B = \frac{2\sigma n_2}{m} \sin(\alpha_2 - \phi) \cos\phi, \tag{28}$$

where n_2 is the index of refraction of the DCG. In the $\phi = 0$ case, the Bragg wavelength and the Littrow wavelength (eq. [12]) are the same. Inserting the above into the grating equation, one can determine the angle of diffraction of the Bragg wavelength to be

$$\sin\beta_B = n_2 \sin\left[\arcsin\left(\frac{\sin\alpha}{n_2}\right) - 2\phi\right]. \tag{29}$$

Because this angle is different from that for the Littrow wavelength, the ghost can be moved off of the detector by introducing a sufficiently large fringe tilt (positive or negative), such that $\Delta\beta \equiv |\beta_L - \beta_B| = |\alpha - \beta_B|$ is greater than the relevant fraction of the camera field of view.

The upper panel of Figure 6 shows the relationship between $\Delta\beta$ and ϕ, which is nearly linear and roughly independent of α. At angles of α up to 45° and $n_2 \sim 1.4$, the small angle approximation for the sin and arcsin are quite good, and we can write $\beta_B \simeq \alpha - 2n_2\phi$. So, for a given α, the fringes need to be tilted by $\phi \simeq \Delta\beta/2n_2$ to move by $\Delta\beta$ degrees away from the position of the Littrow ghost. The sense of the approximation is conservative; for larger α, this formula gives an overestimate for the necessary fringe tilt.

For long-slit spectrographs, $\Delta\beta$ should be at least half the camera FOV, or, as mentioned in § 4.1.1, enough to move the ghost into a detector gap. For RSS and the Bench Spectrograph, the camera FOVs are 16° and 9.8°, requiring $\phi \geq 2.8°$ and $\phi \geq 1.7°$, respectively, for $n_2 = 1.4$, to move the ghost off of the detector over the full range of conceivable incident angles. These are very modest tilts.

To ensure that all ghosts are removed for multiobject spectrographs, the $\Delta\beta$ should be larger, to exclude the ghosts from off-axis objects. For RSS, an additional ~5° needs to be accommodated, resulting in $\phi \geq 4.6°$. However, for configurations with small grating angles ($\alpha \lesssim 20°$), a tilt of the fringes this large moves β_B within a half camera FOV of $\beta_B = 0$, the condition for the appearance of the narcissistic ghost.[16] This may be resolved by tilting the fringes in the negative direction, which moves β_B in the opposite sense. Fringe tilts in either direction have an impact on performance in terms of the merit functions we described above. Hence, a careful consideration of Littrow-ghost removal, avoidance of the introduction of the narcissistic ghost, and impact on performance merit functions must be considered and properly balanced for one's given science goals.

Figure 7 shows the resolution merit function and the anamorphic factor (resolution-element merit function) calculated at the Bragg wavelength versus grating incidence angle for positive and negative fringe tilts. Negative fringe tilts give a small amount of increased resolving power at a given α by significantly increasing dispersion, which overcomes an increase in the anamorphic magnification. However, this means that the detector is less efficiently used, because of the fewer number of resolution elements. Negative fringe tilts also limit the usable range of α for which $\beta_B < 90°$ (transmission), and thus the maximum achievable resolving power in transmission is lowered.

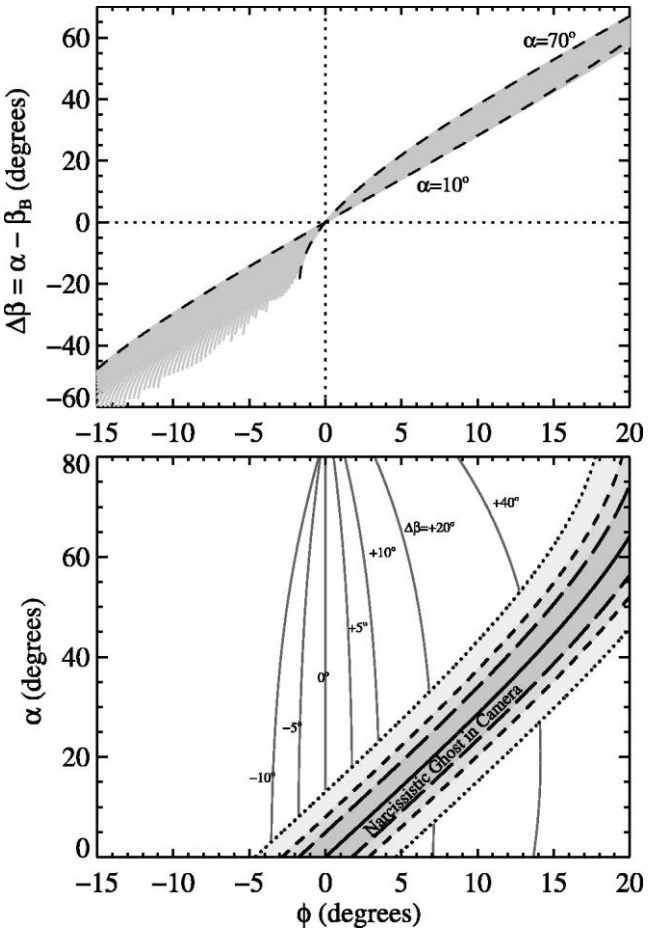

FIG. 6.—Critical angles in tilted-fringe VPH gratings. *Top*: Difference in β between Littrow and Bragg wavelengths for VPH gratings with tilted fringes as a function of fringe tilt, ϕ. The relation is nearly linear and roughly constant with α. Two values of α are overplotted (*dashed lines*), with intermediate range of α filled in gray. When $\Delta\beta \sim \alpha$, the narcissistic ghost enters the camera. *Bottom*: Incidence angle α vs. fringe tilt. Shaded regions show where a fringe tilt would place the narcissistic ghost on the detector for a given α and ϕ, assuming the grating is used at the Bragg angle. The thick solid line is for $\beta_B = 0$, and the others for $\beta_B = 0 \pm \delta$ for the Bench Spectrograph (*long-dashed line*), *RSS* (*short-dashed line*), and RSS-MOS (*dotted line*). Thin solid lines show constant $\Delta\beta$ for a range of values. A tilted-fringe VPH grating should be used over a range of α that avoids the shaded region. Sufficiently negative fringe tilts avoid the narcissistic ghost completely.

[16] The $\beta = 0$ condition occurs when $\phi = \frac{1}{2}\arcsin[(\sin\alpha)/n_2] \approx \alpha/2n_2$.

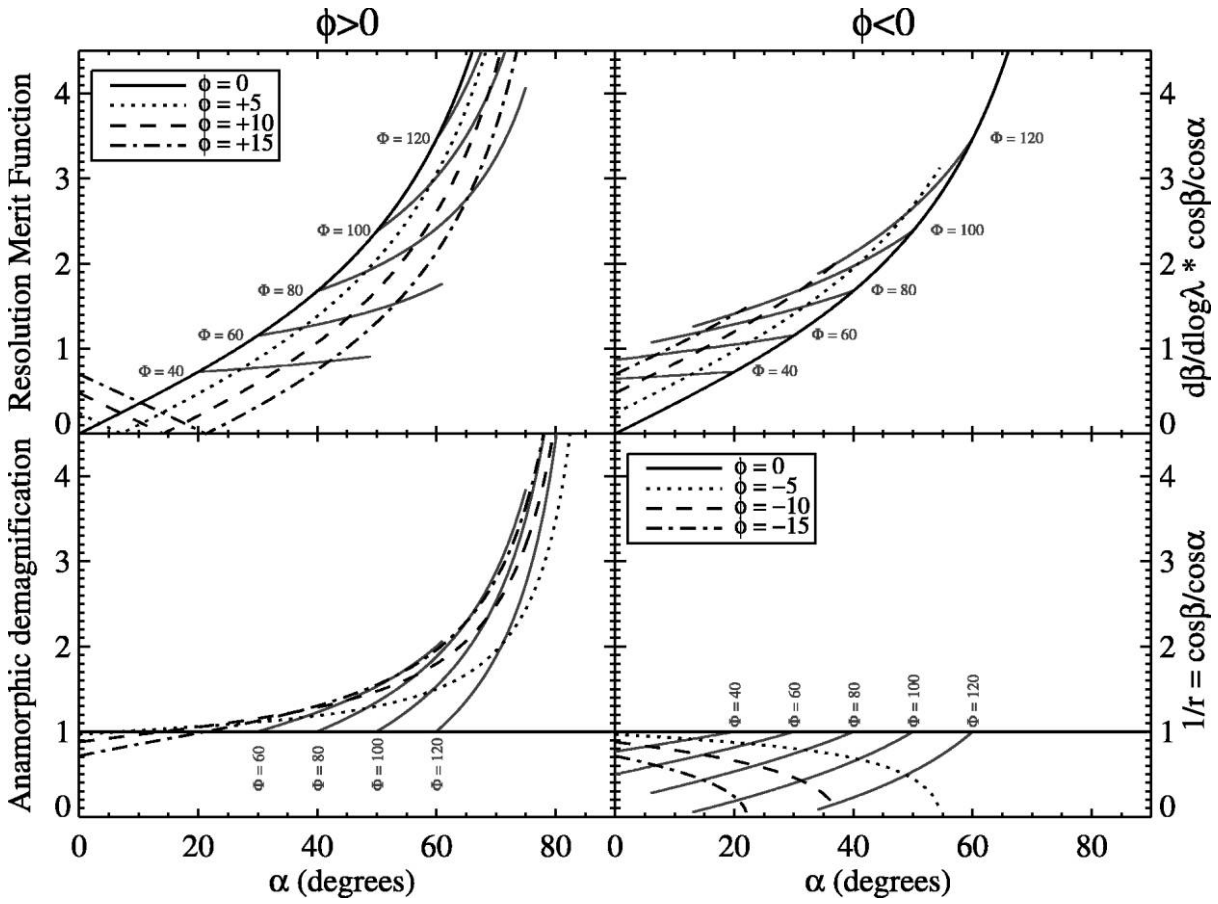

FIG. 7.—Resolution merit function and anamorphic factor evaluated at the Bragg wavelength for plane-parallel VPH gratings with tilted fringes and a mean DCG index $n_2 = 1.4$. Left panels are for $\phi > 0$, and right panels are for $\phi < 0$. Lines of constant camera-collimator angle, $\Phi = \alpha + \beta$, are shown in gray. For a fixed Φ, gratings with positive fringe tilts decrease β, such that the accompanying increase in α can produce significant enhancements in the performance metrics. However, at small α, negative fringe tilts enhance the resolving power with only modest losses in spectral coverage due to increased anamorphic magnification, while preventing the introduction of narcissistic ghosts.

With positive fringe tilts, the anamorphic demagnification ($1/r$) increases strongly at large incidence angles (lower left panel of Fig. 7), although there is little gain for $\phi > 15°$. Note that the demagnification becomes <1 (i.e., magnification) roughly when $\alpha \sim n_2\phi$. This is when the effective diffraction angle ($\alpha_2 - \phi$) changes sign with respect to the tilted fringes (the grating remains in transmission). The overall resolving power decreases with increased positive fringe tilt, but the decrease is modest for small tilt angles. However, the large increase in anamorphic demagnification increases the number of resolution elements, for a definite gain in information. The loss in resolving power can easily be recovered by increasing α and modulating σ in the grating design to tune the wavelength.

In summary, for gratings used at small angles ($\alpha \lesssim 20°$) with wide-field spectrographs, modest negative fringe-tilts should be used to remove Littrow ghosts. Negative tilts will avoid narcissistic ghosts, and boost the resolution merit function via increased dispersion, with some loss in spectral coverage due to increased anamorphic magnification. The other option, namely to use positive fringe tilts large enough to avoid narcissistic ghosts, will also remove Littrow ghosts, but does not do as well in terms of performance metrics for these low angles. At larger α it is beneficial to choose positive tilts in terms of the merit functions. Because of the narcissistic ghosts, however, the tilt must be chosen carefully with the range of α in mind (see Fig. 7, *bottom*).

4.2.2. Prism-Immersed Gratings

In the previous section we considered a VPH grating sandwiched between plane-parallel substrates. By sandwiching the grating between prisms, the grating incident angle, as well as the camera-collimator angle, may be reduced for a given grating and wavelength. The reduction of these angles is favorable because air-glass interface losses are smaller at lower incident

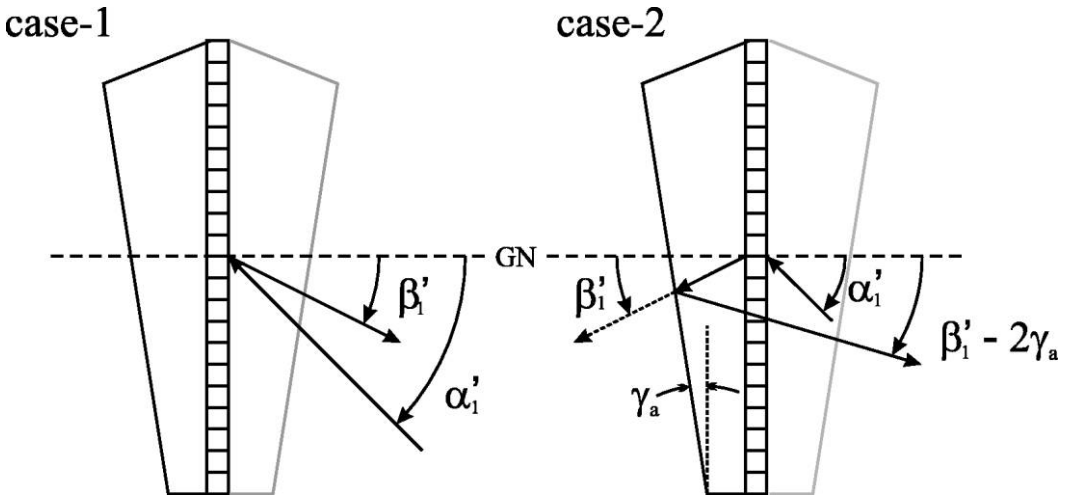

FIG. 8.—Light paths for the case 1 reflective (*left*) and case 2 transmissive (*right*) recombinations in a prism-immersed VPH grating. Only the internal angles are shown. The transmissive recombination ghost is redirected by twice the collimator-side prism angle, γ_a. The internal angles are related to the external angles by $\sin \beta_0 = n_1 \sin (\beta_1 - \gamma_b)$.

angles, and there will be physical constraints on the camera-collimator angle of many spectrographs.

Figure 5 shows the geometry for a general prism-immersed VPH grating, with prism angles γ_a on the collimator side and γ_b on the camera side of the grating. The total beam deviation will be $\alpha_0 + \beta_0 + \gamma_a + \gamma_b$. In the case of untilted fringes, $\phi = 0$, the merit function reduces to

$$\frac{1}{r}\frac{d\beta}{d \log \lambda} = \frac{\cos (\alpha_1 - \gamma_a)}{\cos \alpha_0} 2n_1 \tan \alpha_1, \qquad (30)$$

consistent with equation (A8) of Baldry et al. (2004). It should be noted that this holds true regardless of the value of γ_b, not just for the symmetric case.

Because of the angle of the prism on the collimator side, the beam from the transmissive recombination will be redirected on reflection so that it does not follow the same path as the Littrow wavelength. This manifests itself as a change in β_1 such that $\beta_1^T = \beta_1 - 2\gamma_b$ (see Fig. 8). However, the path of the reflective recombination ghost will remain unchanged. Thus, the use of prism-immersed gratings will not completely resolve the ghost issue, as evidenced by the existence of the ghost in VPH grism spectrographs. The only way to remove the reflective recombination ghost from the camera is to operate the grating itself, i.e., the DCG, in an off-Littrow configuration, as in the tilted fringe case discussed in the previous section.

5. SUMMARY

VPH gratings are becoming much more common in astronomical spectrographs. Despite the clear advantages of using VPH gratings, the necessity of employing a Littrow configuration for gratings with untilted fringes produces an optical ghost that may overlap sensitive sections of the primary spectrum. We have identified two paths for the Littrow ghost with VPH gratings, involving light reflected off of the detector surface that is recollimated by the camera and recombined by the grating before being sent back to the detector. The efficiencies of the two paths depend on the specific properties of the grating and/or antireflection coating of the grating substrates, but even with low efficiency, the great enhancement by full recombination of the $\Delta m = 0$ case produces a ghost that can be as bright as or brighter than the features in the direct spectrum on which it lands.

We have created a theoretical model for the general phenomenon of this ghost that is capable of explaining the observations made by the VPH spectrographs designed and built by the University of Wisconsin–Madison and other institutions, as well as those made with conventional surface-relief gratings. We have shown that our model is capable of accurately reproducing the ghost brightness as observed with reasonable assumptions about the spectrograph and grating performances.

For existing VPH grating spectrographs, there are multiple options to mitigating the effects of the ghost, including changes to the baseline spectrograph configuration or dithering between images—either by changing the spectrograph configuration or by repointing the telescope to move the source along the slit. The extent to which any of these solutions is desirable will depend on the science goals of the observation, as well as the specific spectrograph and telescope limitations.

Although these solutions may be straightforward for the case of single-object long-slit observations, the removal of the effects of the ghost for multiobject, fiber-fed, and nod-and-shuffle modes may be complicated. In MOS modes, telescope nods will be limited because of the typically short lengths of the

individual slits, so unless the sources are small and dominate the ghost flux, it may be best to dither the grating/camera angle. For fiber-coupled systems it will be difficult to move extended sources (covering multiple fibers, e.g., in an IFU) properly along the pseudoslit unless careful attention has been paid to the telescope-to-spectrograph focal-surface mapping. The nod-and-shuffle procedure is typically used for observations of background-limited sources. In this case, the ghost will essentially be similar to a sky line, albeit without line curvature, and as such is as readily removed as the other sky lines.

For future VPH spectrographs, we discussed solutions for removing the ghost completely with new grating designs. We considered both prism-immersed gratings and plane-parallel gratings with tilted fringes. We conclude that the latter is superior because of its ability to remove the ghosts from both the generation paths we have identified. We have analyzed the impact of tilted-fringe gratings in terms of merit functions for spectral resolution and spectral information, whose product is equivalent to the comprehensive measure of "spectral power" (Bershady 2007). We find that modest fringe tilts of $\pm 5°$–$15°$, sufficient to remove Littrow ghosts, can significantly improve spectrograph performance. While some care is needed in the grating design, such that the intended range of user angles (α) avoids the introduction of narcissistic ghosts, the gains are particularly impressive for systems with limited articulation. For example, a fringe-tilt of only 5° for RSS yields up to 80% more spectral power than the existing, untilted gratings. This tilt is sufficiently modest that even with the concerns noted by Rallison & Schicker (1992) about the effects from sag during DCG processing, it is reasonable to expect that there will be little to no negative impact on performance. Furthermore, the incident angles remain small enough ($\alpha \lesssim 60°$) for high-performance AR coatings. The framework presented here should allow the community to usher in a new wave of VPH gratings free of ghost artifacts and boosted in spectral performance by factors of 50% to several 100%.

We would like to thank Patrick Morrissey for pointing out the possibility of the transmissive recombination method for the ghost, and Gary Bernstein for providing his RCWA code and advice on computing reflection modes. Gratitude is also due to Mike Smith, the chief mechanical engineer for the RSS; Sam Gabelt, Don Michalski and the staff of SAL; the University of Wisconsin Physics Department machine shop; the SAAO staff for their work on the RSS detector subsystem; Charles Harmer, Di Harmer, Gene McDougall, Pat Knezek, George Jacoby, Gary Poczulp, and Skip Andre at WIYN/NOAO for technical support; and Sam Barden for initiating the NOAO VPH program and for his critique of this paper in the review stage. We also thank Wasatch Photonics (R. Rallison and D. Cifelli) and CSL (P.-A. Blanche, P. Lemaire, and S. Habraken) for their efforts making science-grade gratings for astronomical application. M. A. B. and K. B. W. were supported by NSF/AST-0307417 and NSF/AST-0607516.

REFERENCES

Baldry, I. K., Bland-Hawthorn, J., & Robertson, J. G. 2004, PASP, 116, 403
Barden, S. C., Armandroff, T., Massey, P., Groves, L., Rudeen, A. C., Vaughnn, D., & Muller, G. 1993, in ASP Conf. Ser. 37, Fiber Optics in Astronomy II, ed. P. M. Gray (San Francisco: ASP), 185
Barden, S. C., Armandroff, T., Muller, G., Rudeen, A. C., Lewis, J., & Groves, L. 1994, Proc. SPIE, 2198, 87
Barden, S. C., Arns, J. A., Colburn, W. S., & Williams, J. B. 2000, PASP, 112, 809
Bershady, M. A. 2007, in 3-D Spectroscopy in Astronomy, ed. E. Mediavilla et al. (Cambridge: Cambridge Univ. Press), in press
Bershady, M. A., Andersen, D. R., Verheijen, M. A. W., Westfall, K. B., Crawford, S. M., & Swaters, R. A. 2005, ApJS, 156, 311
Burgh, E. B., Nordsieck, K. H., Kobulnicky, H. A., Williams, T. B., O'Donoghue, D., Smith, M. P., & Percival, J. W. 2003, Proc. SPIE, 4841, 1463
Jones, D. H., et al. 2004, MNRAS, 355, 747
Joyce, R. R. 2003, GNIRS System Design Note SDN 003.28 (Tucson: NOAO), http://www.noao.edu/ets/gnirs/SDN0003.28.pdf
Kobulnicky, H. A., Nordsieck, K. H., Burgh, E. B., Smith, M. P., Percival, J. W., Williams, T. B., & O'Donoghue, D. 2003, Proc. SPIE, 4841, 1634
McCandliss, S. R., McPhate, J. B., & Feldman, P. D. 1998, Appl. Opt., 37, 5070
Moharam, M. G., & Gaylord, T. K. 1983, J. Opt. Soc. Am., 73, 1105
Rallison, R. D., & Schicker, S. R. 1992, Proc. SPIE, 1667, 266
Saunders, W., et al. 2004, Proc. SPIE, 5492, 389
Smith, M. P., Nordsieck, K. H., Burgh, E. B., Percival, J. W., Williams, T. B., O'Donoghue, D., O'Connor, J., & Schier, J. A. 2006, Proc. SPIE, 6269, 62692A